Late Cenozoic Volcanism in the Hövsgöl Rift Basin: Source, Genesis, and Evolution of Intraplate Volcanism in Mongolia

Honors Thesis
Presented to the College of Agriculture and Life Sciences, Physical Sciences
of Cornell University
in Partial Fulfillment of the Requirements for the
Research Honors Program

by
Andrew V. Zuza
May 2011
Christopher Andronicos

Abstract:

Diffuse, intraplate volcanic deposits are prevalent throughout Mongolia. This study sought to examine Late Cenozoic lavas (9.5-17.1 Ma) from the Hövsgöl rift basin in order to better understand their source, genesis, and evolution. The relationship of these volcanic rocks to the Baikal Rift Zone (BRZ) and the extent to which these lavas are involved in, or derived from, rifting has important implications for lithospheric development of Mongolia and Central Asia. The alkaline basalts have similar light rare earth element enrichments (La/Yb = 9.1-31.9) and $^{87}Sr/^{86}Sr$ ratios in the range of .7039 to .7050. Major and trace element and isotopic data reveal that low degrees of partial melting of garnet lherzolite occurred at depths greater than 65 km. Enrichment in fluid-mobile elements (e.g. Sr and Ba), lower La/Nb ratios, and a calc-alkaline trend suggest that hydrous minerals may have contributed to the melt. Nb enrichment (>35 ppm), along with the melting of hydrous minerals, may be attributed to the melting of a metasomatically enriched lithospheric mantle source. The mixing of minor asthenospheric upwelling with a volatile-rich, metasomatized lithospheric mantle may have produced melts without requiring extremely elevated temperatures, consistent with other published studies that show a small, shallow thermal anomaly under Mongolia.

INTRODUCTION

Late Cenozoic intraplate volcanism is prevalent throughout Mongolia and Central Asia (Fig. 1). Though relatively widespread, volcanic fields are small in volume. The general proximity of these lavas to the Baikal rift zone (BRZ) has led many researchers to regard these as rift-related volcanic rocks, which leads to an important question: what is the relationship between the volcanic rocks and rifting? This question has important implications for the nature of the BRZ itself. Is it an *active* rift, initiated and driven by forces related to mantle convection (see Logatchev and Zorin, 1992; Gao et al., 1994; Zorin et al., 2006), a *passive* rift, with tectonic extension occurring because of far-field forces from the India/Eurasia collision (see Zonenshain and Savostin, 1981; Petit et al., 1997; Nielsen and Thybo, 2009), or some combination of the two (see Petit et al., 1996; Delvaux et al., 1997; Zorin et al., 2003)? A key test to these various hypotheses is the geochemical signatures of the volcanic rocks.

Lake Hövsgöl (referred to as Khubsugul in some literature), which sits in a north-south trending rift basin on the southwestern leg of the BRZ, has numerous exposures of volcanic rocks. This region is a great laboratory for examining the different hypotheses because it is the youngest and most recently active rift basin in the BRZ (Devyatkin and Smelov, 1980). Initial volcanism in the Hövsgöl area (21.4 Ma to 6.17 Ma: Rasskazov et al., 2000) predates extension and crustal rifting (~ 5 Ma: Fedotov et al., 2003) by more than 15 Myr. This fact may argue against *active* rifting, but further study is necessary.

Regardless of the origins of volcanism and rifting, this study aims to examine the geochemical characteristics of these volcanic rocks to better understand their source, genesis, and evolution. The relationship of these volcanic rocks to rifting and the extent to which these lavas

are involved in, or derived from, rifting has important implications for lithospheric development of Mongolia and Central Asia.

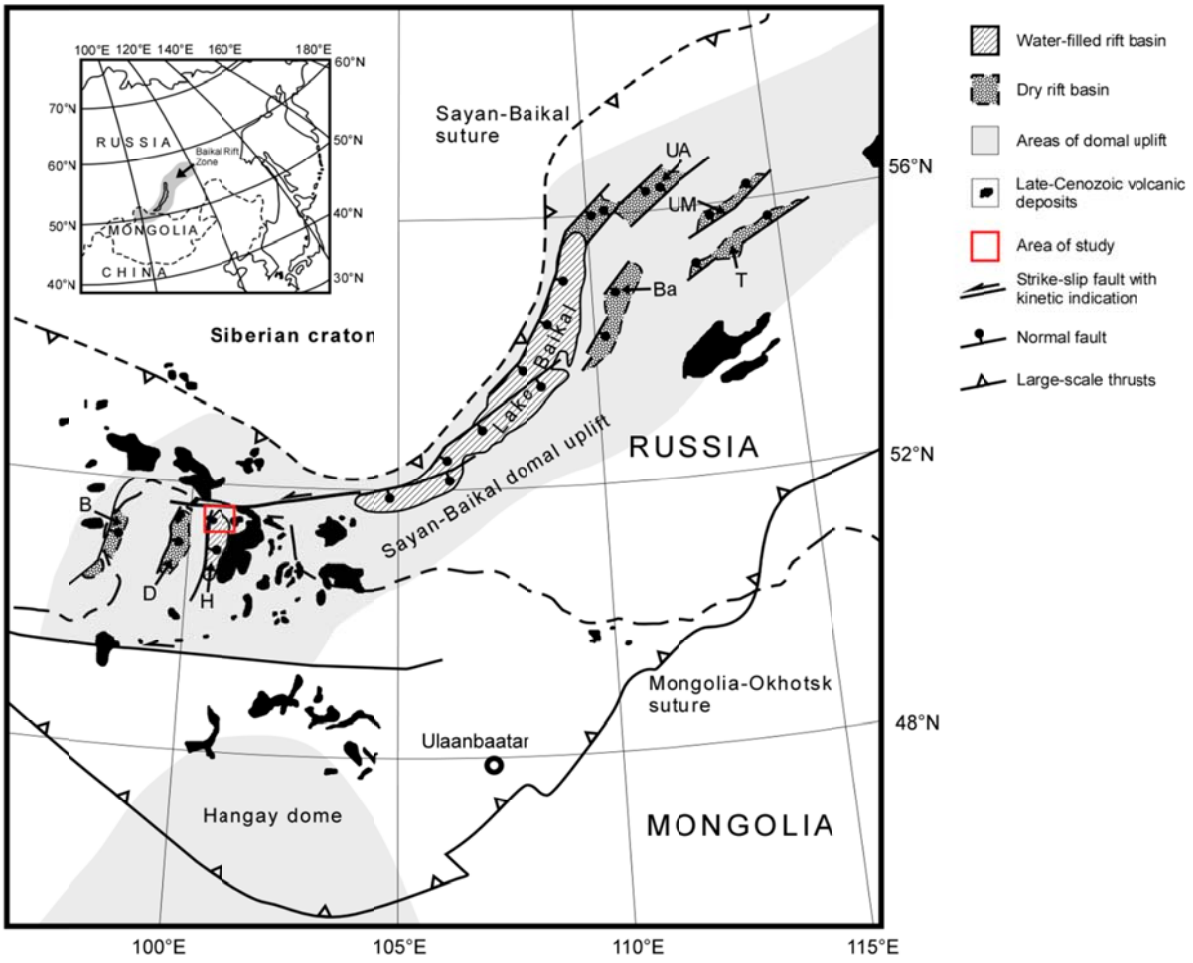

Figure 1. Tectonic map of the Baikal Rift Zone in Southeastern Siberia and Northern Mongolia. Rift basins: B—Busingol, D—Darhat, H—Hövsgöl, UA—Upper Angara, Ba—Barguzin, UM—Upper Muya, and Ts—Tsypa. Complied and modified from Zorin et al. (2003) and Ionov (2002).

GEOLOGIC BACKGROUND

The Baikal rift zone stretches over 1,500 km as a series of Late Cenzoic half-grabens (Zorin, 2003). This rift sequence extends over the southeastern portion of the Siberian craton (Fig. 1). The rift is spatially controlled by the location of lithospheric plate and microplate boundaries, only cutting through older basement structures in the most northeastern section

(Mats, 1992). The rift half-grabens of the BRZ are asymmetric, with master faults forming on the Siberian craton side of the rift at all localities except for two rift-basins in the northeast (Fig. 1). The earliest rift volcanism in the BRZ occurred in the Late Cretaceous-Paleogene (80-35 Ma: Rassakov, 1994), preceding the onset of extension and the subsequent formation of rift basins in the Oligocene (30-35 Ma: Logatchev, 1993). Volcanism was most active in the Middle-Late Miocene and in the Pliocene-Quaternary (Rassakov, 1994).

Many rift basins have formed along the length of the BRZ, including the Hövsgöl, Darhat, Baikal, and Barguzin basins. The Hövsgöl rift is believed to be the youngest of three parallel, N-S orientated grabens on the southwestern fringe of the BRZ (Devyatkin, 1980). Extension within the Hövsgöl rift started later than that of the main Baikal Rift, beginning ~ 5 Ma (Fedotov et al., 2003).

The Hövsgöl rift basin is located at the suture between the Tuva-Mongolian massif and several Paleozoic terranes (Rasskazov et al., 2000a). The Tuva-Mongolian massif is a complex of Neoproterozoic terranes. Two of these terranes are formally recognized: a continental block and an island arc, known as the Gargan microcontinent and the Dunzhugur island arc respectively (Kuzmichev et al., 2001). These terranes were incorporated onto the Siberian craton via large-scale thrusts in the Late Ordovician-Silurian as part of the Sayan-Baikal orogenic belt. Three Paleozoic metamorphic terranes, which were amalgamated onto the Sayan-Baikal orogenic belt, are exposed on the eastern edge of the Hövsgöl rift basin. The Tunka and Khamar-Daban terranes are believed to be metamorphosed back-arc basins (Shkol'nik, 2008), whereas the Dzhida terrane is a metamorphosed island-arc (Al'mukhamedov et al., 1996).

From the Late Permian to the Late Jurassic the continental margin consisted of the Mongol-Okhotsk Ocean (Kravchinsky et al., 2002). A subduction zone and a Late Paleozoic arc formed, intruding granitic magma into the overlying Gargan microcontinent (Zorin et al., 1995). The Mongol-Okhotsk Ocean began to close in the Late Jurassic (Kravchinsky et al., 2002), eventually forming the southwest-northeast trending Mongol-Okhotsk suture (Fig. 1; see synthesis by Yin, 2010). Units of both the Gargan microcontinent and Late Paleozoic granitoids crop out on the northwestern side of Lake Hövsgöl, whereas rocks of the Paleozoic metamorphic terranes are found to the northeast of the lake (Fig. 2).

The Late Cenozoic basalts that are the focus of this study lie unconformably on top of these basement rocks. Volcanic deposits in the Hövsgöl area (21.4 Ma to 6.17 Ma: Rasskazov et al., 2000) are faulted by extensional and crustal rifting processes during the Late-Miocene (<5 Ma: Fedotov et al., 2003). Quaternary fluvial, lacustrine, and glacial sedimentary deposits cover much of the area around Lake Hövsgöl.

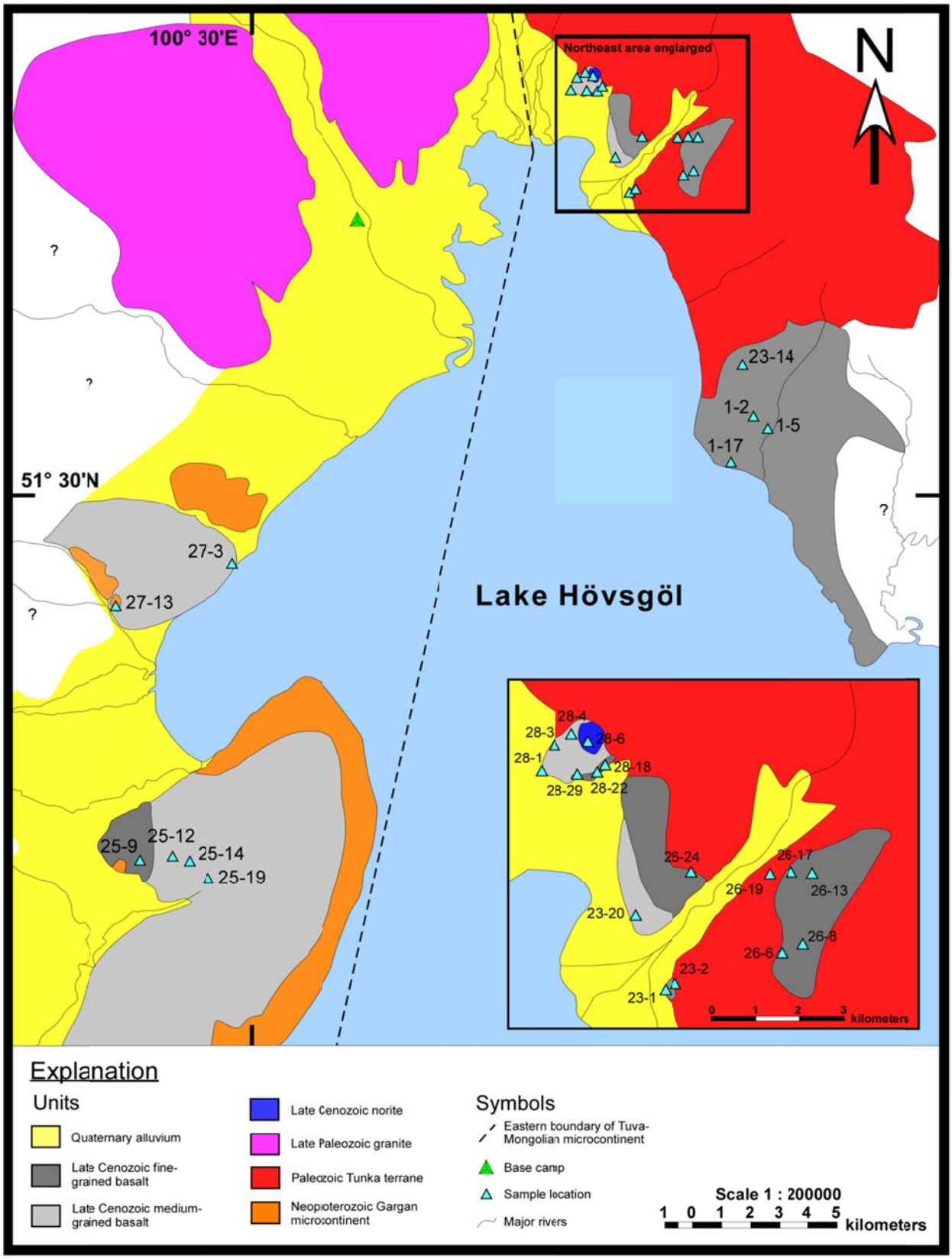

Figure 2. Geologic map of the northern region of Lake Hövsgöl. Dashed line marks microcontinent boundary, from Zorin et al. (2003).

METHODS

A month of field work was conducted during the summer of 2010. The ~400 km^2 field area was mapped at a scale of 1:200,000. Twenty-eight basalt samples were collected and were made into singly polished thin sections by Texas Petrographic Services Inc. Twenty-four bulk-rock samples were crushed and powdered for geochemical work. Major and minor element analysis was conducted at the Cornell Center for Materials Research on 20 of the samples using a JEOL-8900 microprobe on glasses made from fused whole-rock powders. Instrumental neutron activation analysis (INAA) was utilized to examine the trace elements of 16 representative samples. Bulk rock powder (~.5 g) was sealed in silica glass ampoules. Samples were irradiated by the Nuclear Reactor Program at North Carolina State University and later analyzed in an ORTEC GEM-20170-S solid-state γ-ray spectrometer at Cornell University. Sr isotope ratios were analyzed for 12 samples using a FISONS VG Sector 54 Thermal Ionization Mass Spectrometer (TIMS) at Cornell University's W. M. Keck Foundation Isotope Laboratory. Data are reported in Table 1 (standard analysis are given in Table A1 and A2).

Table 1: Major and trace element compositions of Hövsgöl basalts

Region:	West				Northeast							
Sample:	27-3	25-14b	27-1	25-12	25-9	28-29	28-3	28-6	28-1	28-4	28-18	23-14a
Major and minor elements (wt%)												
SiO_2	47.98	49.10	48.58	49.65	-	45.58	51.67	50.97	46.85	-	46.19	-
TiO_2	2.36	2.32	2.15	2.27	-	3.05	2.32	3.44	2.23	-	2.90	-
Al_2O_3	13.83	15.79	16.72	15.42	-	14.52	15.61	16.51	14.51	-	14.66	-
FeO	11.61	10.39	11.65	9.93	-	11.81	9.55	9.45	11.20	-	11.62	-
MnO	0.21	0.17	0.16	0.19	-	0.18	0.12	0.13	0.17	-	0.16	-
MgO	11.51	8.12	5.72	7.88	-	7.72	7.12	3.02	8.28	-	7.34	-
CaO	7.59	8.83	10.22	8.72	-	8.27	7.39	7.25	7.86	-	7.57	-
Na_2O	2.61	3.12	3.30	3.11	-	3.59	3.89	4.83	3.45	-	3.77	-
K_2O	1.96	1.67	0.87	1.87	-	2.13	2.13	3.04	1.80	-	2.67	-
P_2O_5	0.65	0.53	0.41	0.62	-	0.69	0.43	0.88	0.51	-	0.99	-
Total	100.32	100.03	99.79	99.67	-	97.54	100.23	99.51	96.87	-	97.88	-
Trace elements (ppm)												
La	28.0	25.7	18.7	-	35.9	37.5	-	-	25.2	24.1	-	23.9
Ce	58.8	55.1	41.5	-	73.0	78.7	-	-	53.3	53.1	-	51.7
Nd	34.0	26.8	21.2	-	40.7	38.5	-	-	31.8	27.9	-	28.8
Sm	6.25	5.93	4.85	-	7.61	8.28	-	-	6.27	6.37	-	6.40
Eu	2.04	2.02	1.91	-	2.50	2.60	-	-	1.98	2.19	-	2.08
Tb	0.84	0.89	0.94	-	0.94	1.06	-	-	0.85	1.01	-	0.91
Yb	1.55	1.37	2.06	-	1.13	1.22	-	-	1.46	1.47	-	1.57
Lu	0.196	0.179	0.2816	-	0.143	0.148	-	-	0.182	0.179	-	0.195
Sr	736	808	427	-	924	1576	-	-	634	762	-	663
Ba	372	316	509	-	382	387	-	-	388	364	-	390
Cs	0.2	0.2	0.2	-	0.3	0.4	-	-	0.3	0.4	-	0.3
U	0.7	0.5	-	-	0.9	1.5	-	-	0.8	0.9	-	0.7
Th	2.4	2.0	0.9	-	3.2	3.7	-	-	2.6	2.4	-	2.4
Hf	4.0	4.0	3.3	-	4.7	5.9	-	-	4.7	5.0	-	4.7
Ta	2.6	2.3	1.0	-	3.7	3.9	-	-	2.8	2.8	-	2.7
Sc	16.6	17.7	27.6	-	12.3	13.3	-	-	16.2	16.0	-	17.0
Cr	190	204	120	-	106	116	-	-	221	186	-	191
Ni	147	100	36	-	113	127	-	-	110	90	-	96
Co	57	43	33	-	42	45	-	-	48	42	-	45
Isotopic ratios												
$^{87}Sr/^{86}Sr$	0.70461	0.70432	0.70499	-	0.70394	0.70600	-	-	0.70453	0.70474	-	-

Table 1: continued

Region:	Northeast								East			
Sample:	23-20	23-2	26-19	26-8	26-24	26-17	26-6	26-13	23-1	1-2	1-17	1-5
Major and minor elements (wt%)												
SiO_2	-	50.82	50.27	50.14	48.09	49.02	48.60	48.87	49.62	50.54	50.74	49.62
TiO_2	-	2.24	2.54	2.41	2.45	2.41	2.62	2.43	2.18	2.37	2.46	2.05
Al_2O_3	-	15.03	15.10	14.88	15.01	15.03	14.92	15.16	15.56	15.48	15.71	15.22
FeO	-	11.50	10.58	10.48	11.22	10.21	11.25	10.53	10.05	9.54	9.59	10.02
MnO	-	0.17	0.15	0.15	0.15	0.18	0.16	0.16	0.14	0.16	0.14	0.17
MgO	-	7.53	7.49	7.77	7.26	7.66	7.31	7.26	6.72	6.77	5.95	8.46
CaO	-	7.71	8.07	7.82	7.86	8.02	7.66	7.87	8.06	7.48	7.66	7.72
Na_2O	-	3.42	3.83	3.45	3.63	3.70	3.30	3.68	3.82	3.31	4.46	3.51
K_2O	-	1.56	1.78	1.62	1.96	1.75	1.84	1.57	1.66	2.02	2.41	1.45
P_2O_5	-	0.55	0.54	0.45	0.53	0.39	0.56	0.45	0.56	0.56	0.69	0.43
Total	-	100.54	100.35	99.15	98.16	98.36	98.21	97.97	98.37	98.22	99.82	98.65
Trace elements (ppm)												
La	24.6	-	20.7	20.1	24.0	-	26.9	22.0	-	24.687	-	20.562
Ce	53.7	-	43.9	44.2	51.3	-	48.8	27.2	-	50.625	-	43.943
Nd	27.0	-	26.7	24.0	28.5	-	27.0	26.7	-	23.456	-	20.869
Sm	6.09	-	5.60	5.59	6.55	-	7.07	6.27	-	5.481	-	5.178
Eu	2.03	-	1.86	1.90	2.07	-	1.95	1.97	-	1.810	-	1.752
Tb	0.91	-	0.82	0.88	0.96	-	0.91	0.94	-	0.780	-	0.750
Yb	1.43	-	1.43	1.39	1.40	-	1.48	1.56	-	1.174	-	1.148
Lu	0.179	-	0.182	0.177	0.18	-	0.183	0.189	-	0.148	-	0.140
Sr	679	-	594	679	643	-	658	703	-	665.333	-	915.408
Ba	415	-	340	320	363	-	391	342	-	386.077	-	311.939
Cs	0.7	-	0.2	0.3	0.3	-	0.2	0.3	-	0.291	-	0.246
U	0.8	-	0.5	0.7	0.7	-	0.7	0.7	-	1.099	-	0.662
Th	2.6	-	1.9	1.9	2.4	-	2.2	2.1	-	2.825	-	1.779
Hf	4.6	-	3.9	4.0	4.9	-	4.4	4.4	-	3.888	-	3.384
Ta	2.6	-	2.2	2.1	2.8	-	2.7	2.4	-	2.167	-	1.674
Sc	15.9	-	16.6	16.3	15.5	-	15.1	17.3	-	12.9	-	13.9
Cr	200	-	188	194	178	-	180	202	-	151	-	230
Ni	96	-	109	121	98	-	133	128	-	102	-	133
Co	42	-	42	43	43	-	42	45	-	34	-	41
Isotopic ratios												
$^{87}Sr/^{86}Sr$	0.70458	-	-	0.70449	0.70461	-	-	0.70443	-	-	-	0.70487

FIELD RELATIONS

Lava flows crop out extensively in the northern region of Lake Hövsgöl (Fig. 2), ranging from highly eroded relicts to well preserved flows that can be examined in cross-section (Fig. 3a, b). In these sections, rubbly aa flow tops are visible, with massive lava deposits underneath, often with sheared vesicles (Fig. 3a). Brecciated bottoms or the presence of paleosols demarcate the bottom of individual flows (Fig. 3b). Flow thickness generally ranges from 1 to 5 m, and the

largest vertical section had at least 6 stacked basalt flows. Basement rock structures and fabrics generally trend NNE-SSW, perpendicular to regional extension.

Samples are grouped into three spatial regions—west, northeast, and east—for analysis and discussion. The flows were also compared with similar volcanic deposits 10 km east of the lake (i.e. Heven Plateau: Perepelov et al., 2010).

Dating of the flows by Rasskazov et al. (2000) show that the west and north east flows are 9.5 $\pm$ .3 Ma (K-Ar) and 10.2 $\pm$ .5 Ma (K-Ar), respectively. The eastern flows are 16.44 $\pm$ .08 Ma ($^{40}Ar/^{39}Ar$: Rasskazov et al., 2000) and the Heven Plateau flows are 17.1 $\pm$ .4 Ma ($^{40}Ar/^{39}Ar$: Perepelov et al., 2010).

PETROGRAPHY

The samples are silica undersaturated, alkali basalts. Olivine phenocrysts are abundant in all but one sample. Olivine composition is generally 85-90% forsterite (+ optic sign and 2V $\approx$ 90°). Olivine often exhibits normal zoning (i.e Mg-rich cores with more Fe-rich rims). Clinopyroxene and plagioclase are also sometimes zoned. Minor alteration is present in many of the samples, with small amounts of olivine weathering to iddingsite (Fig. 3d). Some olivine is also rimmed by pyroxene. Generally, textural growth patterns reveal expected mineralization sequences, with olivine and calcium-rich plagioclase crystalizing before the pyroxenes and less calcic plagioclase.

Northeast flows

Samples from the northeast have the most diverse range of textures. A portion of these samples represent an extrusive lava flow. They are finer-grained and porphorytic, dominated by euhedral olivine phenocrysts. These samples have an aphanitic ground mass populated by

plagioclase microlites, which sometimes have a preferred orientation, presumably controlled by flow direction. Some samples have larger plagioclase phenocrysts, indicating slower cooling rates or plagioclase fractionation in the magma chamber. Some clinopyroxene (modal 5-15%) and orthopyroxene (modal 5-10%) phenocrysts exist.

Other samples have undergone slower cooling, and are medium-grained, with a phaneritic texture. They are made up of predominately euhedral to subhedral olivine, plagioclase, and clinopyroxene, with lesser amounts of orthopyroxene. Plagioclase often exhibits trachytic textures (Fig. 3e). Textural growth patterns reveal that Ca-rich plagioclase crystallized first (Fig. 3f), followed by olivine and intermediate plagioclase, and then clinopyroxene (Fig. 3g).

The last volcanic lithology identified in the region is phaneritic large grained (>5 mm) norite. This lithology has a relatively sharp contact with the medium-grained deposits that were discussed above (Fig. 3c). There is no olivine present in these samples, with the rock composed of clinopyroxene, orthopyroxene, and plagioclase feldspar. There are also long (~5mm), preferentially oriented ilmenite crystals. The plagioclase feldspar is the intermediate to calcic labradorite (%An ~55%). The labrodorite commonly grows around the clino- and orthopyroxenes, although some synchronous growth is evident.

These three lithologies are likely part of the same flow (Fig. 2), with the fine grained rocks representing the chilled margin.

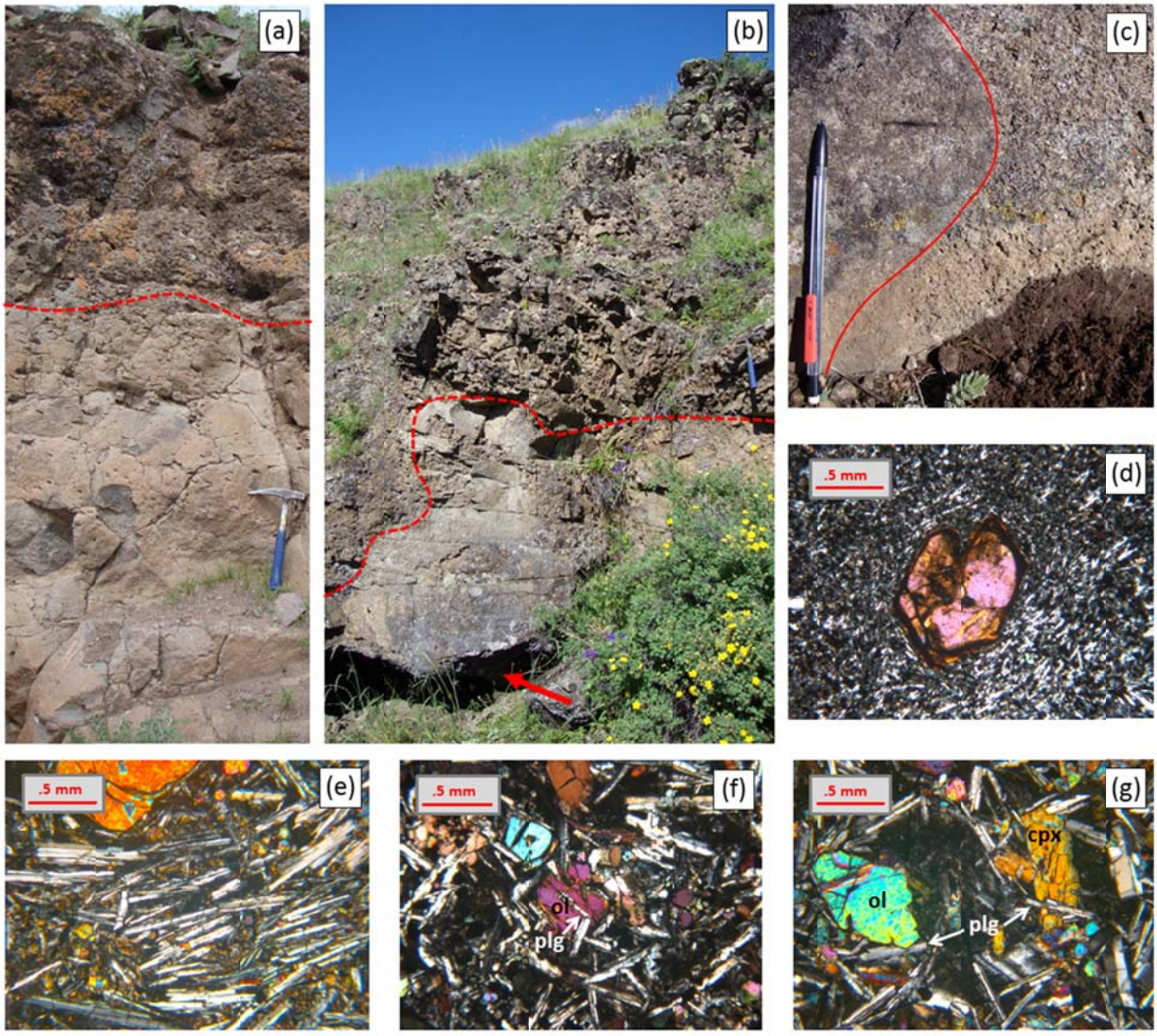

Figure 3. Typical flows (a, b) in cross section, showing rubbly aa top flow and more massively bedded flow interior, separated by red dashed line. Hammer for scale. Sheared vesicles are present (a) in massive beds. Eroded paleosols (b), indicated by red arrow, are often present at the base of individual flows; (c) Contact between medium-grained and coarse-grained basalts; Photomicrographs showing (d) euhedral olivine weathering to iddingsite, (e) trachytic texture of plagioclase, (f) olivine growing around plagioclase, and (g) clinopyroxene growing around plagioclase, with plagioclase growing around olivine.

West flows

Samples from the western region display less variety than those in the northeast. Some have a fine-grained to glassy matrix with fine grained plagioclase, with olivine phenocrysts. Other medium-grained samples contain euhedral plagioclase and olivine, commonly with olivine

growing around plagioclase (Fig. 3f). Subhedral to anhedral clinopyroxene and orthopyrxene are also present, but are modally less abundant.

East flows

These flows are glassier, with more groundmass by volume. Overall, these flows appear different from the other two regions, dominated almost solely by olivine euhedral to subhedral phenocrysts. Rare clinopyroxene phenocrysts exist.

GEOCHEMISTRY

Major and minor elements

Major element analysis reveals that a majority of the lavas in this region are basalt or trachy-basalt, with lesser amounts of basaltic trachyandesite and tephrite basanite (Fig. 4a: total-alkali-silica classification scheme of Le Bas et al., 1986). All of the samples are alkaline (Fig. 4a: Le Bas et al., 1986). They are basic (45.6-51.0 wt % SiO_2), and have MgO wt % ranging from 5.7 to 11.5 (Table 1). The lavas follow a calc-alkaline trend on an AFM plot (Fig. 4b: Irvine and Baragar, 1971).

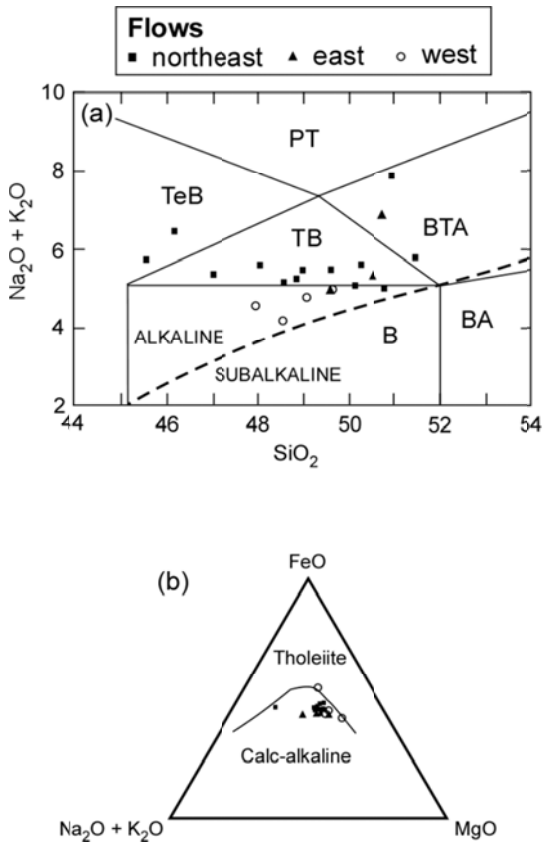

Figure 4. (a) Total alkalis ($Na_2O + K_2O$) vs SiO_2 relative to the TAS classification scheme of Le Bas et al. (1986), where B—basalt, TB—trachybasalt, TeB—tephrite basanite, PT—phonotephrite, BTA—basaltic trachyandesite, and BA—basaltic andesite. (b) AFM plot ($Na_2O + K_2O$ – FeO – MgO tertiary) following Irvine and Baragar (1971).

Plots of SiO_2, K_2O, and FeO versus MgO show substantial scatter (not shown), and limited trends exists in plots of CaO/Al_2O_3, Al_2O_3, Na_2O, and TiO_2 versus MgO (Fig. 5). With decreasing MgO, CaO/Al_2O_3 also decreases, whereas Al_2O_3 increases. This suggests that the fractionation of clinopyroxene, which incorporates more CaO than Al_2O_3, is important for the evolution of these magmas. Na_2O and TiO_2 generally increase with decreasing MgO, although the correlation is faint. The sample with the largest-grain size is most evolved (~3 wt % MgO) and has the highest TiO_2 (3.44 wt %), consistent with occurrence of ilmenite crystals.

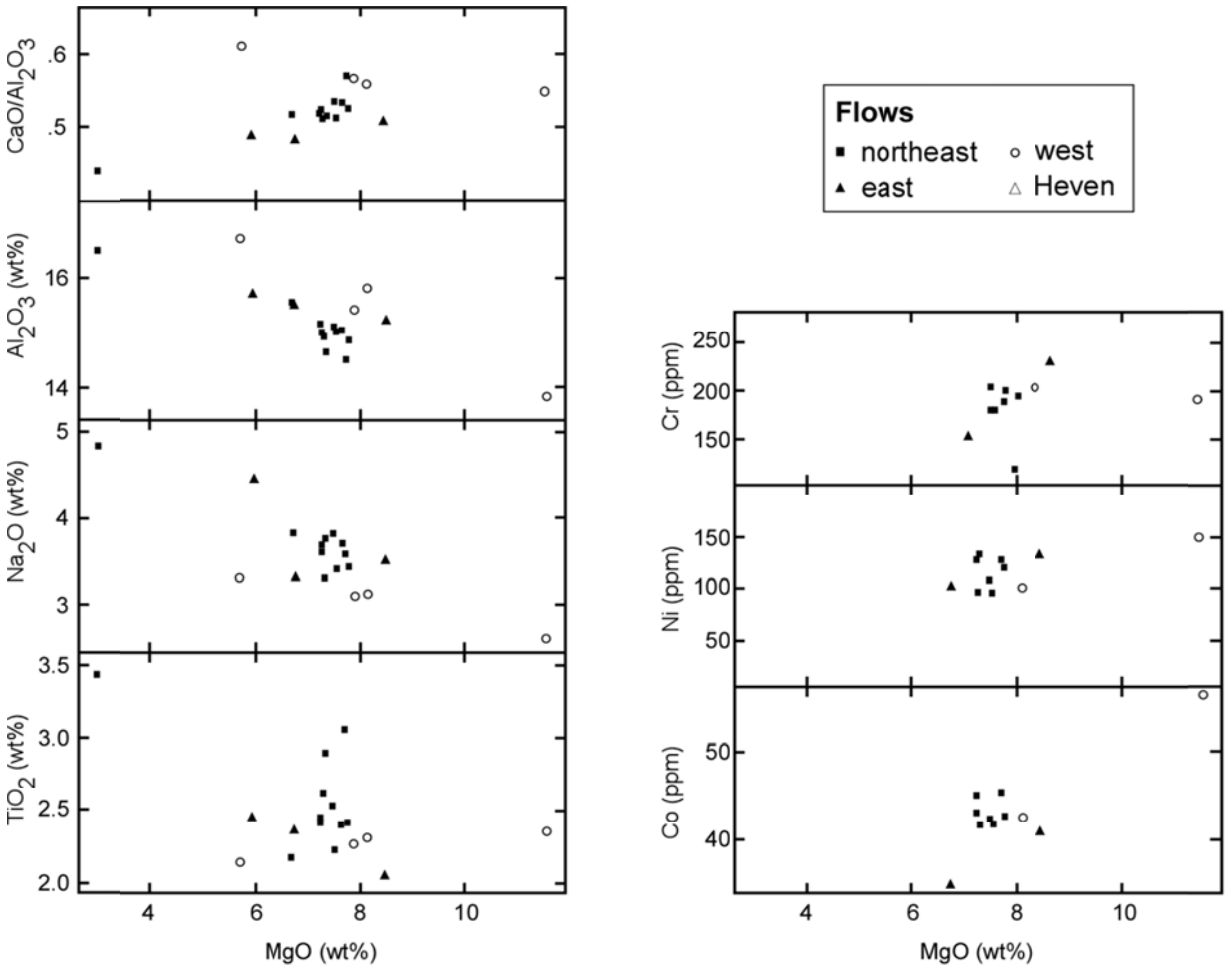

Figure 5. Variation diagrams of MgO vs CaO/Al_2O_3, Al_2O_3, Na_2O, TiO_2, Cr, Ni, and Co.

Trace elements

These lavas, as well as those at Heven Plateau (Perepelov et al., 2010), have similar primitive mantle-normalized trace element patterns (Fig. 6), and are enriched in incompatible trace elements. The lavas have steep rare earth element (REE) patterns, are enriched in light rare earth elements (LREE) relative to heavy rare earth elements (HREE), and are generally similar to ocean island basalts (OIB). Compatible elements (e.g. Cr, Ni, and Co) generally decrease with decreasing MgO (Fig. 5), suggesting that the fractionation of olivine and clinopyroxene is important in differentiating these magmas. Cr vs. MgO has the strongest trend of the trace elements, with Ni and Co having only faint trends.

There are notable negative Th anomalies in all of the samples, and slight positive Ba and Sr anomalies in many samples. Ba/La ratios are slightly higher than those found in OIB (Fig. 7). On a plot of La/Ta versus Ba/Ta (Fig. 7), the samples fall between lavas from the Rio Grande rift (i.e. lithospheric source: Thompson et al., 2005) and from Hawaii (i.e. plume source: Watson, 2003).

The volcanic deposits at Heven Plateau have similar LREE enrichment (La/Yb = 20.6-21.6) relative to the flows on the east (La/Yb = 17.9-21.0), suggesting a similarity between these deposits. The lavas from the northeast have slightly less LREE enrichment (La/Yb = 14.1-30.8), and the western flows have varied LREE enrichment (La/Yb = 9.1-31.9). The La/Yb ratios of the northeastern and western flows overlap, supporting similarity.

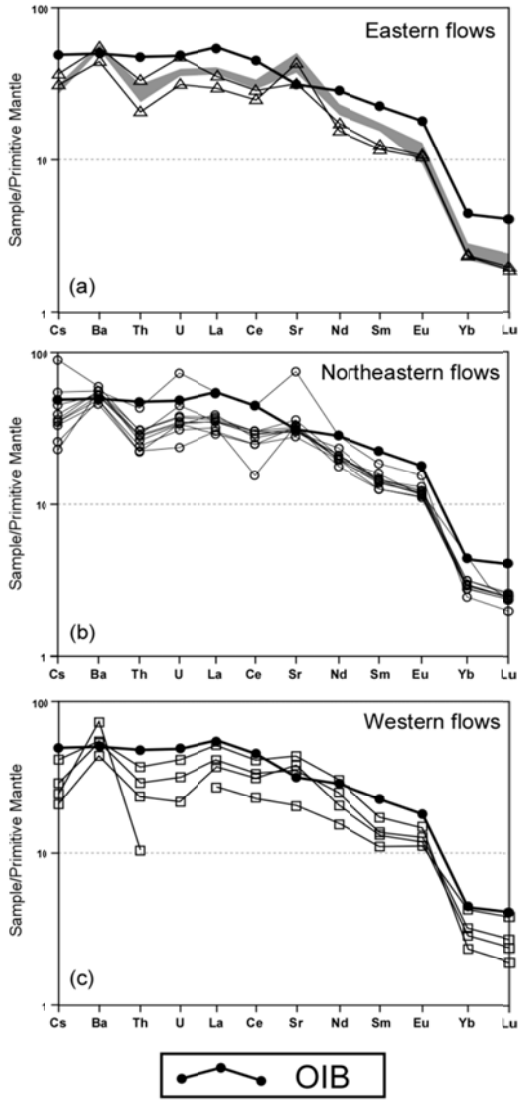

Figure 6. Primitive mantle-normalized trace element patterns for (a) eastern, (b) northeastern, and (c) western field locations. Shaded line represents lavas from the Heven Plateau. Heven Plateau data from Perepelov et al. (2010). OIB and primitive mantle compositions from Sun and McDonough (1989).

Strontium isotopes

All but one of the analyzed samples have $^{87}Sr/^{86}Sr$ ratios in the range of .7039 to .7050, and the outlier sample has a ratio of .7060 (Table 1). The ratios fall between the two end-member OIB-source types—HIMU ($^{87}Sr/^{86}Sr$ = .7029) and EM1 ($^{87}Sr/^{86}Sr$ = .705)—suggesting a mixing of source types (Sun and McDonough, 1989). The average ratio value of around .7047 is

most similar to EM1. The occurrence of an anomalously high $^{87}Sr/^{86}Sr$ ratio (.7060) is discussed later.

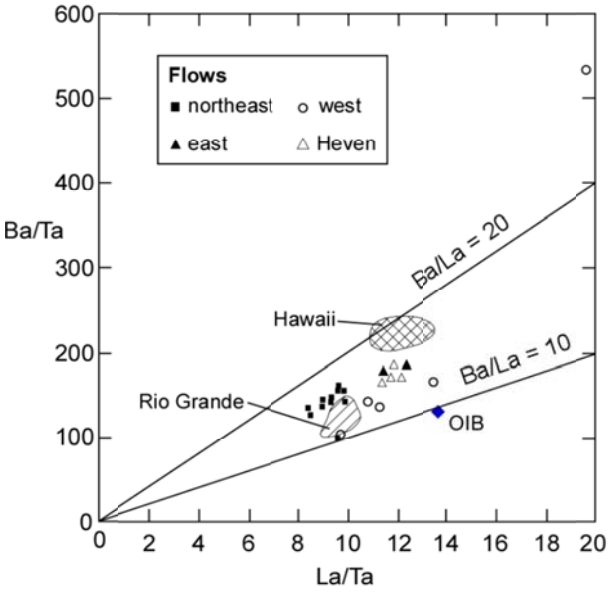

Figure 7. La/Ta vs. Ba/Ta for Hövsgöl and Heven Plateau samples (Perepelov et al., 2010). OIB composition from Sun and McDonough (1989), Hawaii compositions from Watson (2003) and Rio Grande compositions from Thompson et al. (2005).

DISCUSSION

Crustal contamination

Mantle-derived lavas should be analyzed to evaluate the extent of crustal contamination. The samples have low Th/La and $^{87}Sr/^{86}Sr$ ratios, which is evidence against upper crustal contamination. The samples are not depleted in Ta and they do not trend toward continental crust or marine sediment influence on a plot of Nb*/U vs. Th/La (Fig. 8).

Barry et al. (2003) showed that the lower and middle crust in the region has higher $^{87}Sr/^{86}Sr$ ratios (>.705) and Sr concentrations. Only one sample has values this high ($^{87}Sr/^{86}Sr$ ratio = .706 and Sr = 1576ppm), possibly indicating crustal contamination, although the lack of

other significant variations for other major and trace elements may point toward laboratory contamination during sample preparation.

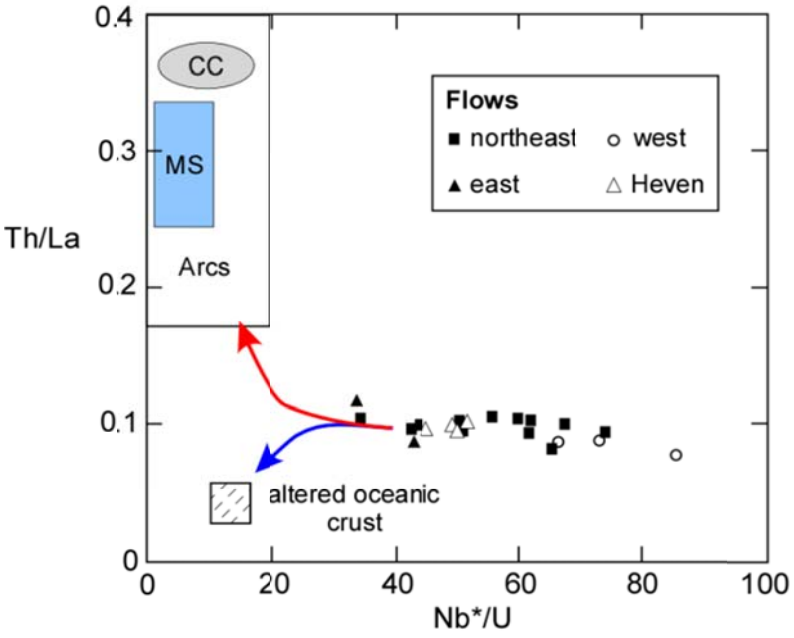

Figure 8. Nb*/U vs. Th/La for Hövsgöl and Heven Plateau samples (Perepelov et al., 2010), where Nb* = 17 × Ta (Sun and McDonough, 1989). Red arrows shows projected influence of continental crust, arcs, or marine sediments on melt, and blue arrow shows projected influence of altered oceanic sediments. Continental crust (CC) from Rudnick and Fountain (1995). Arcs, marine sediment (MS), and altered oceanic crust compositions are from Klein and Karsten (1995).

Fractional crystallization

The low MgO (5.7-11.5%) contents of these lavas indicate that they are not the product of primary melts, suggesting some shallow crustal-level fractionation and differentiation of a parental melt. The compositional trends of these lavas can partly be explained by the fractional crystallization of observed olivine and clinopyroxene phenocrysts. Olivine phenocrysts are observed in all but one sample, with clinopyroxene present in most. The trend of decreasing CaO/Al_2O_3 with decreasing MgO (Fig. 5) suggests that the fractionation of clinopyroxene plays a significant role in differentiating the magma. Low MgO (5.7-11.5%), Cr (106-230 ppm), and Ni (36-147 ppm), as well as the trends of Cr, Ni, and Co versus MgO (Fig. 5), verify the importance of olivine and clinopyroxene fractionation. The fractionation of plagioclase was less important,

as plagioclase would have taken both CaO and Al_2O_3 out of the melt, which is not seen as MgO decreases (Fig. 5). The lack of a negative Eu anomaly (Fig. 6) also supports this.

The considerable scatter (Fig. 5) with these trends suggests that fractionation of a single parental melt cannot be entirely responsible for the compositional differences of these samples. Magma mixing, high-pressure fractionation (see Barry et al., 2003), or a varied source may account for the observed compositional differences.

Melt source

Steep REE patterns (La/Yb ~ 15-30) suggest that melting occurred within the garnet lherzolite stability field (Fig. 6, 9). The spinel-garnet transition zone in the region is located at ~65 km depth (Ionov et al. 1998), providing a minimum depth for melt production. Other investigations on Mongolian basalts have shown magma generation depths greater than 70 km (Barry et al., 2003; Perepelov et al., 2010). The relationship between Ba/Ta and La/Ta (Fig. 7), $^{87}Sr/^{86}Sr$ ratios (most .7039-.7050), and minimal crustal interaction suggest that melting occurred at the base of the lithosphere or in the uppermost asthenosphere.

Geochemical evidence (Fig. 9), pressure/temperature constraints at $\geq$ 65 km depth, and other studies (e.g. Barry et al., 2003) suggest that a low degree of partial melting produced these magmas. Anhydrous melting at these depths would require extremely elevated asthenospheric mantle temperatures, which are not observed in geophysical surveys (Poort and Klerkx, 2004). P-T analyses on garnet lherzolite xenoliths also indicate that the lower lithosphere does not have temperatures greater than 1100^0C (Ionov et al., 1998). The existence of volatiles could produce melts at these lower temperatures.

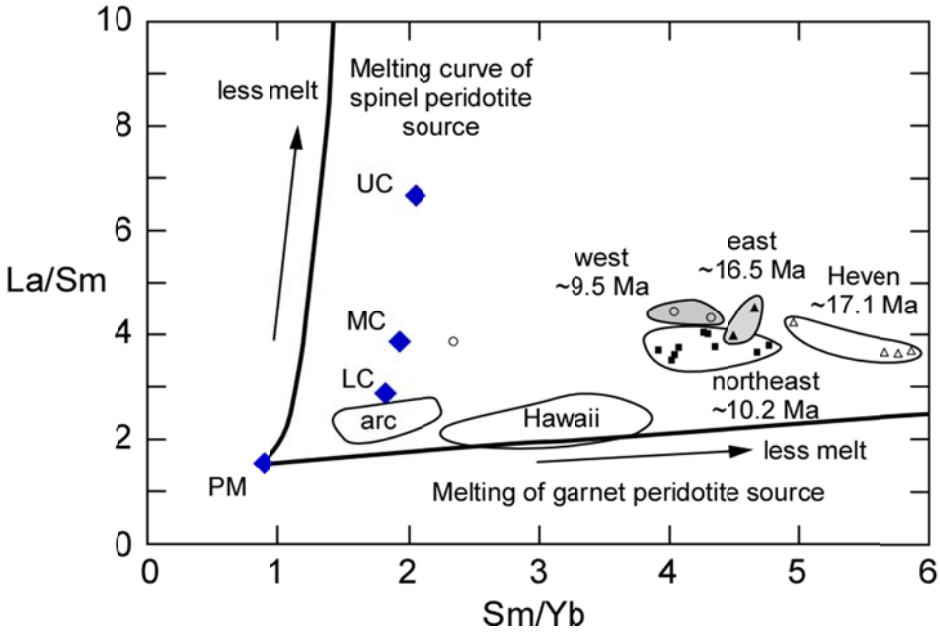

Figure 9. Sm/Yb vs. La/Sm for Hövsgöl and Heven Plateau samples (Perepelov et al., 2010). Shown for comparison are arc rocks (Kay et al., 1993) and Hawaiian basalts (Lassiter and DePaolo, 1997). Primitive mantle (PM) composition from Sun and McDonough (1989) and lower crustal (LC), middle crustal (MC), and upper crustal (UC) compositions from Rudnick and Fountain (1995). Batch melting curves show characteristics of magmas derived from smaller degrees of partial melting of spinel peridotite and garnet peridotite sources, based on Lassiter and DePaolo (1997). Dates are from Rasskazov et al. (2000).

Enrichment in fluid-mobile elements (e.g. positive Sr and Ba anomalies: Fig. 6) and low La concentrations (Table 1; Fig. 10) suggest that hydrous minerals may have contributed to the melt. As pointed out by Sun and McDonough (1989), lower La/Nb and $^{87}Sr/^{86}Sr$ ratios may show that the melting source interacted directly or indirectly with altered recycled oceanic crust (e.g. an old slab). The lavas have low values for these ratios, falling off the trend for typical OIB melts (Fig. 10). The calc-alkaline trend (Fig. 4b) also suggests some influence of a subducted slab on the melt. A plot of Nb*/U vs. Th/La (Fig. 8) reveals that the melt source was not directly related to altered oceanic crust, as the they do not trend toward direct influence with altered oceanic crust. Th concentrates in oceanic crust, and is relatively immobile, so its strong

depletion in the Hövsgöl lavas (Fig. 6) also confirms that the magmas are not the product slab melting (Klein and Karsten, 1995).

As previously described by Barry et al. (2003), this may suggest the presence of a metasomatized lithospheric mantle source. Sr enrichment is associated with the melting of amphibole and Ba enrichment can be associated with the melting of phlogopite (Fig. 6). Metasomatic enrichment of the lithosphere would provide such hydrous minerals. High Nb* (i.e. 17 × Ta: Sun and McDonough, 1989) enrichment (>35 ppm) also supports this idea, as high Nb concentrations may be derived from metasomatized lithospheric mantle (Stein and Kessel, 1997).

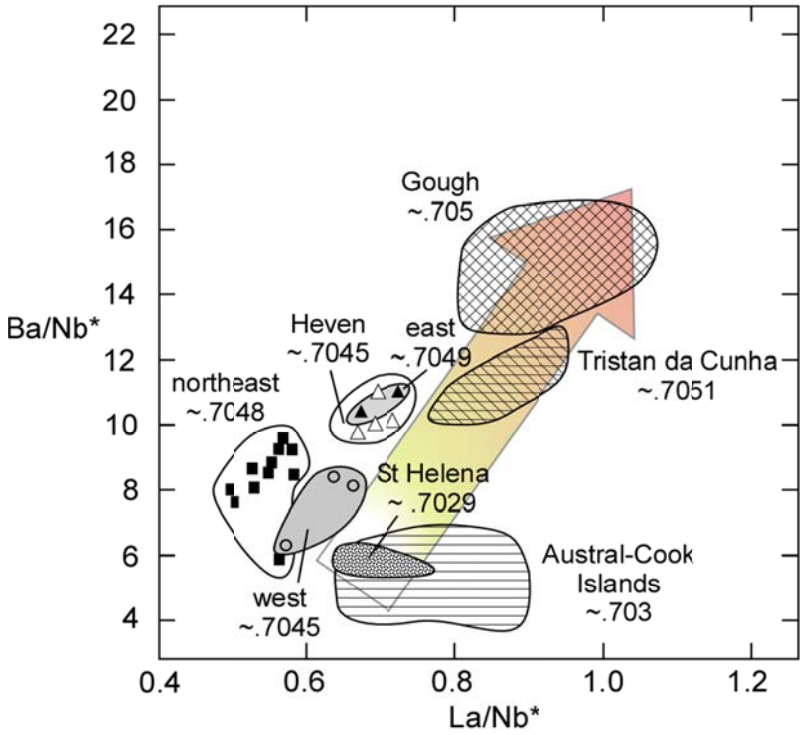

Figure 10. (a) La/Nb* vs. Ba/Nb* for Hövsgöl and Heven Plateau samples (Perepelov et al., 2010), where Nb* = 17 × Ta (Sun and McDonough, 1989). Arrow represents typical positive correlation between the linear relationship of Ba/Nb and La/Nb ratios and increasing $^{87}Sr/^{86}Sr$ ratios of OIB, as described by Sun and McDonough (1989). Gradation in arrow depicts transition between the HIMU-type (white) and EM1-type (red) OIB sources. Numerical values represent $^{87}Sr/^{86}Sr$ ratios. Ratios for St. Helena, Tristen de Cunha, and Gough are modified from Weaver et al. (1986) and data from Austal-Cook Islands from Panter et al. (2006).

Metasomatism

A possible model for the metasomatic enrichment in this region involves the Paleozoic Mongol-Okhotsk subduction zone (Zorin, 1999). Panter et al. (2006) found similar metasomatic enrichment related to ancient subduction in New Zealand and Marie Byrd Land, where fluid-mobile elements and enriched fluids migrated from the dehydrating slab to the base of the overlying lithosphere. The base of the lithosphere inboard of a subduction zone became altered by the products of the dehydrating slab. After subduction ceased, metasomatized lithospheric mantle was formed (Stein and Kessel, 1997). Alkaline magmatism, with similar trace element characteristics, occurred inboard and parallel to an ancient subduction zone. Similar enrichment may have occurred in the Hövsgöl region. The Mongol-Okhotsk Ocean closed at the end of the Mesozoic, forming the southwest-northeast trending Mongol-Okhotsk suture (see synthesis by Yin, 2010). Lake Hövsgöl is inboard of this suture, in the region where subduction-related metasomatism could have occurred (Fig. 1).

This volatile-rich, metasomatized lithospheric mantle may have sat until activated by a thermal anomaly to trigger partial melting and magmatism. This may help to explain why Late Cenozoic magmatism is not specifically related temporally or spatially to rift basins (e.g. minimal volcanism near Lake Baikal: Fig.1; Zorin et al., 2003), but rather, is parallel to the Mongol-Okhotsk suture. Arc-related, Late Paleozoic granites crop out in the Hövsgöl region (Fig. 2), indicating that the area is a reasonable distance from the proto-subduction zone to have undergone enrichment from the dehydrating slab.

Magma genesis and evolution

Even with the lowered melting temperature associated with a volatile-rich metasomatized lithospheric mantle, a thermal source is still required to initiate melting. Shallow asthenospheric upwelling, seen as a slight thermal anomaly beneath Mongolia (Zhao, 2001), may have triggered melting. $^{87}Sr/^{86}Sr$ ratios (most .7039-.7050: average of .7047) support this, suggesting the mixing of EM1-like (i.e. enriched asthenosphere) with HIMU-like (i.e. a metasomatized mantle) source (Sun and McDonough, 1989). The lack of a deep-rooted low velocity zone suggests that this minor upwelling is not derived from great depth (Zhao, 2001). Several explanations for shallow asthenospheric upwelling have been suggested: (1) thermal blanketing by the Eurasia continent, leading to small amounts of convection (Barry et al., 2003); (2) lithospheric delamination and subsequent replacement by the asthenosphere (Barry et al., 2003); or (3) the sinking of subducted oceanic slabs, resulting in an upwelling asthenosphere (Yin, 2010). A combination of these processes may be occurring.

The results of this study, as well as others (e.g. Barry et al., 2003; Perepelov et al., 2010), indicate that Late Cenozoic volcanism in this region has been relatively continuous and similar for over 20 Myr. Incompatible element patterns and isotopic ratios for the flows analyzed in this study, which span ~8 Myr, show little variation (Fig. 6, 7, 8). This fact, along with a gradual increase in the degrees of partial melting over time (Fig. 9), may suggest that asthenospheric upwelling is related to thermal blanketing of the region by a thickened mantle lithosphere (Yin, 2010). Following this model, terrane amalgamation and the gradual development of Central Asia since the Neoproterozoic has greatly thickened the lithosphere (Rasskazov et al., 2000a; Yin, 2000; Barry et al., 2003). This large Eurasian continental mass may be leading to a thermal blanketing effect, with small asthenospheric convective cells developing in response to a slow

warming of the upper mantle. Other models for asthenospheric upwelling (e.g. deep-rooted plume or delamination) would likely show more temporal and chemical variations.

CONCLUSIONS

Petrographic and geochemical analysis of Late Cenozoic lavas from the Hövsgöl rift basin was conducted in order to determine magma source, genesis, and evolution. Crustal contamination is minimal. Trace elements and isotopic ratios reveal that low degrees of partial melting of garnet lherzolite occurred at depths greater than 65 km. An enriched asthenospheric source probably interacted with a volatile-rich, metasomatized lithospheric mantle, to produce melts without requiring significantly elevated temperatures.

Although previously discounted by Barry et al. (2003), influence and dehydration of the oceanic crust associated with the Paleozoic Mongol-Okhotsk subduction zone seems like a likely mechanism for creating metasomatically enriched lithospheric mantle. Work by Panter et al. (2006) found similar trace element and isotopic ratio signatures for melts of metasomatized mantle lithosphere on the inboard side of ancient sutures, which appears to be a good analogue for Mongolian magmatism.

The cause of asthenospheric upwelling is questionable, although consistent lava compositions over at least 20 Myr and increasing degrees of partial melting with time, may support the model of thermal blanketing by a thickened lithosphere.

In terms of the debate between *active* and *passive* rifting, low-volume volcanism, lack of a deep-rooted low velocity zone (Zhao, 2001), and the temporal disconnect between volcanism and crustal rifting (> 15 Myr: Rasskazov et al., 2000; Fedotov et al., 2003) seem to rule out the

possibility of a mantle plume driving extension. Minor upwelling is likely occurring to trigger melting of a volatile-rich metasomatized source, but it is unlikely that this is causing intra-continental extension. In this region, rifting is likely *passive*, with extension along preexisting structures (e.g. sutures, fabrics, etc.) being controlled by far-field stress.

Further study would benefit from more isotopic information (e.g. Nd and Pb isotopes) and precise dating on these volcanic deposits. This would allow for better constraints of the source and timing of melt generation. Additionally, a broader sampling of volcanic deposits across Mongolia and Central Asia would aid in understanding the regional implications of Late Cenozoic volcanism.

ACKNOWLEDGEMENTS

This project was made possible by the Keck Geology Consortium, with additional support coming from an Cornell University's Engineering Learning Initiatives research grant and a Keck-ExxonMobil Enhanced grant. Suzanne Kay (Cornell University) provided valuable advice and assistance with electron microprobe and INAA analysis. Further laboratory support by Robert Kay (Cornell University), with INAA, and John Hunt (Cornell University), with the electron microprobe work, helped immensely. Tremendous field support and guidance was provided by Aranzal Bat-Erdene (Mongolian University of Science and Technology) and Andrew de Wet (Franklin & Marshall College). Camp logistics and cooking, provided by Sarantsetseg Gonchigdori and Dagiimaa Yadam, made fieldwork possible.

REFERENCES

Al'mukhamedov, A. I., Gordienko, I. V., Kuz'min, M. I., Tomurtogoo, O., and Tomurkhuu, D., 1996, The Dzhida Zone: A Fragment of the Paleoasian Ocean: Geotectonics, v. 30, no. 4, p. 279-294.

Barry, T.L., Saunders, A.D., Kempton, P.D., Windley, B.F., Pringle, M.S., Dorjnamjaa, D., Saandar, S., 2003, Petrogenesis of Cenozoic basalts from Mongolia: Evidence for the role of asthenospheric versus metasomatized lithospheric Mantle Sources: Journal of Petrology, v. 44, p. 55-91.

Devyatkin, Y.V., and Smelov, S.B., 1980, Position of basalts in the Cenozoic sedimentary sequence of Mongolia: International Geology Review, v. 22, p. 307-317.

Delvaux, D., Moeys, R., Stapel, G., Petit, C., Levi, and K., Miroshnichenko, A., Ruzhich, V., and San'kov, V., 1997, Paleostress reconstructions and geodynamics of the Baikal region, Central Asia, Part 2. Cenozoic rifting: Tectonophysics, v. 282, no. 1-4, p. 1-38.

Fedotov, A., San'Kov, V., De Batist, M., Kazansky, A., Parfeevets, A., Miroshnitchenko, A., and Pouls, T., 2006, Chronology of the Baikal Rift System: EOS Transactions. AGU, v. 87, no. 25, p. 246-250.

Gao, S., Davis, P. M., Liu, H. and Slack, P. D., 1994, Asymmetric upwarp of the asthenosphere beneath the Baikal rift zone, Siberia: Journal of Geophysical Research, v. 99, no. B8, p.15319-15330.

Ionov, D. A., O'Reilly, S. Y., and Griffin, W. I., 1998, A geotherm and lithospheric section for Central Mongolia (Tariat region): Mantle Dynamics and Plate Interactions in East Asia – American Geophysical Union Monograph, Geodynamics Series, v. 27, p. 127-153.

Ionov, D. A., 2002, Mantle structure and rifting processes in the Baikal–Mongolia region: geophysical data and evidence from xenoliths in volcanic rocks: Tectonophysics, v. 351, p. 41-60.

Irvine, T. N., and Baragar, W. R. A., 1971, A guide to the chemical classification of the common volcanic rocks: Canadian Journal of Earth Sciences, v. 8, p. 523-548.

Klein, E. M., and Karsten, J. L., 1995, Ocean ridge basalts with convergent margin geochemical affinities from the southern Chile Ridge: Nature, v. 374, p.52-57.

Kravchinsky, V. A., Cogné, J.-P., Harbert, W. P., and Kuzmin, M. I., 2002, Evolution of the Mongol-Okhotsk Ocean as constrained by new palaeomagnetic data from the Mongol-Okhotsk suture zone, Siberia: Geophysical Journal International, v. 148, no. 1, p. 34-57.

Kuzmichev, A. B., Bibikova, E. V., and Zhuravlev, D. Z., 2001, Neoproterozoic (~800 Ma) orogeny in the Tuva-Mongolia Massif (Siberia): island arc–continent collision at the northeast Rodinia margin: Precambrian Research, v. 110, p. 109-126.

Lassiter, J. C. and DePaolo, D. J., 1997, Plume/lithosphere interactions in the generation of continental and oceanic flood basalts: chemical and isotopic constraints: Large Igneous Provinces: Continental, Oceanic, and Planetary Flood Volcanism (Mahoney, J.J. & Coffin, M. F. (eds)). Geophysical Monograph, American Geophysical Union, v. 100, p. 335–356.

Le Bas, M.J., LeMaitre, R.W., Streckeisen, A.L., and Zanettin, B., 1986, A chemical classification of volcanic rocks based on the total alkali-silica diagram: Journal of Petrology, v. 27, p. 745-750.

Logatchev, N.A., 1993. History and geodynamics of the Baikal rift in the context of the Eastern Siberia rift system - a review: Bulletin des Centres de Recherches Exploration, v. 17, p. 353–370.

Logatchev, N.A. and Zorin, Y.A., 1992, Baikal rift zone: Structure and geodynamics: Tectonophysics, v. 208, no. 1-3, p. 273-286.

Nielsen, C. and Thybo, H., 2009, No Moho uplift below the Baikal Rift Zone: Evidence from a seismic refraction profile across southern Lake Baikal: Journal of Geophysical Research B: Solid Earth, v. 114, no. 8, p. 1-22.

Panter, K. S., Blusztajn, J., Hart, S. R., Kyle, P. R., Esser, R., and Mcintosh, W. C., 01, 2006, The Origin of HIMU in the SW Pacific: Evidence from Intraplate Volcanism in Southern New Zealand and Subantarctic Islands: Journal of Petrology, v. 47, no. 9, p. 1673-1704.

Petit, C., Deverchere, J., Houdry, F., Sankov, V. A., Melnikova, V. I., and Delvaux, D.,1996, Present-day stress field changes along the Baikal rift and tectonic implications: Tectonics, v. 15, no. 6, p. 1171.

Petit, C., Burov, E. and Déverchère, J., 1997, On the structure and mechanical behavior of the extending lithosphere in the Baikal Rift from gravity modeling: Earth and Planetary Science Letters, v. 149, no. 1-4, p. 29-42.

Perepelov, A. B., Tsypukova, S. S., Demonterova, E. I., Pavlova, L. A., Travin, A. V., and Bat-Ulzii, D., 2010, The first mineralogical, geochemical, and isotope-geochronological data on neogene alkaline basaltic volcanism of the Heven Zalu Uriin Sar'dag Plateau (Northern Mongolia): Doklady Earth Sciences, v. 434, no. 1, p. 1230-1234.

Mats, V. D., 1993, The structure and development of the Baikal rift depression: Earth Science Reviews. v. 34, no. 2, p. 81-118.

Poort, J., and Klerkx, J., 2004, Absence of a regional surface thermal high in the Baikal rift; new insights from detailed contouring of heat flow anomalies: Tectonophysics, v. 383, no. 3, p. 217 – 241.

Rasskazov S. V., Ivanov A. V., and Demonterova E. V., 2000a, Deep-seated inclusions in Zun-Murin basanites (Tunka rift valley, Baikal region): Russian Geology and Geophysics, v. 41, p. 98-108.

Rasskazov, S.V., Logachev, N.A., Brandt, I.S., Brandt, S.B., and Ivanov, A.V., 2000, Geochronology and geodynamics of the Late Cenozoic in Southern Siberia, Southern and Eastern Asia: Nauka Publications, p. 288.

Rasskazov, S.V., Luhr, J.F., Bowring, S.A., Ivanov, A.V., Brandt, I.S., Brandt, S.B., Demonterova, E.I., Boven, A.A., Kunk, M., Hough, T., Dungan, M.A., 2003, Late Cenozoic Volcanism in the Baikal Rift System: Evidence for Formation of the Baikal and Khubsugul Basins due to Thermal Impacts on the Lithosphere and Collision-Derived Tectonic Stress: Berliner Palaobiologische Abhandlugen, v. 4, p. 33-48.

Shkol'nik, S.I., Reznitskii, L.Z., Belichenko, V.G., and Barash, I.G., 2009, Geochemistry, petrogenesis, and geodynamic typification of metavolcanics of the Tunka terrane (Baikal-Hovsgol region): Russian Geology and Geophysics, v. 50, no. 9, p. 779-788.

Stein, M., Navon, O., and Kessel, R., 1997, Chromatographic metasomatism of the Arabian-Nubian lithosphere: Earth and Planetary Science Letters, v. 152, p. 75-91.

Sun, S., and McDonough, W.F., 1989, Chemical and isotope systematics of oceanic basalts: Implications for mantle composition and processes, In Saunders, A.D.,and Norry, M.J., eds. Magmatism in the ocean basins: Geological Society, London, Special Publication 42, p. 313-345.

Thompson, R. N., Ottley, C. J., Smith, P. M., Pearson, D. G., Dickin, A. P., Morrison, M. A., Leat, P. T., Gibson, S. A., 2005, Source of the Quaternary Alkalic Basalts, Picrites and Basanites of the Potrillo Volcanic Field, New Mexico, USA: Lithosphere or Convecting Mantle?: Journal of Petrology, v. 46, no. 8, p. 1603-1643.

Watson, S., 1993, Rare earth element inversions and percolation models for Hawaii: Journal of Petrology, v. 35, p. 763–783.

Weaver, B.L., Wood, D.A., Tarney, J., and Joron, J.L., 1986, Role of subducted sediment in the genesis of ocean-island basalts: geochemical evidence from South Atlantic Ocean islands: Geology, v. 14, no. 4, p. 275-278.

Yin, An., 2010, Cenozoic tectonic evolution of Asia: A preliminary synthesis: Tectonophysics, v. 488, no. 1, p. 293-325.

Zhao, D., 2001, Seismic structure and origin of hotspots and mantle plumes: Earth and Planetary Science Letters, v. 192, no. 3, p. 251-265.

Zonenshain, L.P. and Savostin, L.A., 1981, Geodynamics of the Baikal rift zone and plate tectonics of Asia: Tectonophysics, v. 76, no. 1-2, p. 1-45.

Zorin, Y.A., Turutanov, E.K., Mordvinova, V.V., Kozhevnikov, V.M., Yanovskaya, T.B. and Treussov, A.V., 2003, The Baikal rift zone: The effect of mantle plumes on older structure, Tectonophysics, v. 371, no. 1-4, p. 153-173.

Zorin, Y.A., Turutanov, E.K., Kozhevnikov, V.M., Rasskazov, S.V. and Ivanov, A.V., 2006, Cenozoic upper mantle plumes in East Siberia and Central Mongolia and subduction of the Pacific Plate: Doklady Earth Sciences, v. 409, no. 5, p. 723-726.

APPENDIX

Table AI: Standards used for INAA

	Known values*			This study (Run 1)*			This study (Run 2)*		
Standard:	WBD	PAL	SIT	WBD	PAL	SIT	WBD[1]	PAL	SIT
FeO[a]	9.59	10.15	4.34	9.59	10.15	4.34	9.59	10.15	4.34
Na_2O[a]	0.11	2.07	5.30	.159	2.04	5.30	.5023	2.03	5.30
La	82.9	10.5	14.6	82.9	10.29	13.64	82.9	10.30	14.37
Ce	158.0	23.6	33.8	158	22.55	32.22	158	22.79	32.96
Nd	58.0	13.0	18.3	58	14.056	19.02	58	12.29	17.62
Sm	8.23	3.42	4.68	8.23	3.31	4.36	8.23	3.32	4.55
Eu	2.14	1.07	1.09	2.17	1.07	1.03	2.16	1.07	1.11
Tb	0.620	0.67	0.760	0.509	0.67	0.68	.469	.67	.750
Yb	0.610	2.18	3.42	0.684	2.18	3.41	.668	2.18	3.41
Lu	0.085	0.304	.500	0.085	0.304	.494	.080	.304	.485
Sr	-	183	255	535.62	226	255	501.30	201	255
Ba	1280	185	935	1186	179.43	935	1171	185.79	935
Cs	1.81	2.19	1.25	1.21	1.99	1.44	1.81	1.96	1.56
U	2.35	0.497	2.58	2.35	.313	2.69	2.35	.464	3.62
Th	11.00	2.07	5.26	11.00	1.94	5.05	11.00	1.98	5.13
Hf	3.92	2.56	4.61	3.92	2.46	4.41	3.92	2.58	4.79
Ta	8.30	0.65	0.54	8.30	0.642	.614	8.30	.622	.626
Sc	20.2	37.5	9.25	20.2	39.11	9.56	20.2	38.52	9.86
Cr	1910	314	2	1910	303.48	.693	1910	306.97	.539
Ni	991	89	2	991	87.65	6.84	991	89.58	9.30
Co	88	53	36	88	53.67	26.41	88	52.42	27.28

*ppm except where indicated
[a] wt %

Table A2: Standards used for electron microprobe analysis

	Known values (wt %)			This study (wt %)		
Standard:	A99	JdF	Kak	A99	JdF	Kak
SiO_2	50.94	50.81	40.37	51.05	50.49	40.54
TiO_2	4.06	1.85	4.72	4.03	1.85	4.76
Al_2O_3	12.49	14.06	14.90	12.61	14.13	14.69
FeO	13.32	11.88	10.92	13.52	11.82	10.82
MnO	0.19	0.22	0.09	0.19	0.21	0.09
MgO	5.08	6.71	12.80	5.01	6.88	12.67
CaO	9.30	11.12	10.30	9.26	11.12	10.34
Na_2O	2.66	2.62	2.60	2.75	2.67	2.60
K_2O	0.82	0.19	2.05	0.83	0.19	2.04
P_2O_5	0.38	0.20	-	0.40	0.19	-
Total	99.24	99.66	98.75	99.65	99.55	98.54